2018

Mechanism of how augmin directly targets the γ-tubulin ring complex to microtubules

Jae-Geun Song

Matthew R. King

Rui Zhang

Rachel S. Kadzik

Akanksha Thawani

See next page for additional authors

Authors
Jae-Geun Song, Matthew R. King, Rui Zhang, Rachel S. Kadzik, Akanksha Thawani, and Sabine Petry

JCB Journal of Cell Biology

ARTICLE

Mechanism of how augmin directly targets the γ-tubulin ring complex to microtubules

Jae-Geun Song[1], Matthew R. King[1], Rui Zhang[2], Rachel S. Kadzik[1], Akanksha Thawani[3], and Sabine Petry[1]

Microtubules (MTs) must be generated from precise locations to form the structural frameworks required for cell shape and function. MTs are nucleated by the γ-tubulin ring complex (γ-TuRC), but it remains unclear how γ-TuRC gets to the right location. Augmin has been suggested to be a γ-TuRC targeting factor and is required for MT nucleation from preexisting MTs. To determine augmin's architecture and function, we purified *Xenopus laevis* augmin from insect cells. We demonstrate that augmin is sufficient to target γ-TuRC to MTs by in vitro reconstitution. Augmin is composed of two functional parts. One module (tetramer-II) is necessary for MT binding, whereas the other (tetramer-III) interacts with γ-TuRC. Negative-stain electron microscopy reveals that both tetramers fit into the Y-shape of augmin, and MT branching assays reveal that both are necessary for MT nucleation. The finding that augmin can directly bridge MTs with γ-TuRC via these two tetramers adds to our mechanistic understanding of how MTs can be nucleated from preexisting MTs.

Introduction

Microtubules (MTs) originate from specific locations in the cell, which are broadly defined as MT organizing centers (MTOCs; Brinkley, 1985; Lüders and Stearns, 2007). MT nucleation at MTOCs requires the γ-tubulin ring complex (γ-TuRC), which provides a ring-shaped template to assemble α, β-tubulin heterodimers into a MT (Moritz et al., 1995; Zheng et al., 1995; Kollman et al., 2011). Therefore, it is essential to target γ-TuRC to these nucleation sites. Several factors have been identified in vivo to play a role in recruiting γ-TuRC to MTOCs, such as AKAP450 at the Golgi apparatus, CDK5RAP2 and NEDD1 at centrosomes, and augmin and NEDD1 at spindle MTs (Haren et al., 2006; Lüders et al., 2006; Fong et al., 2008; Rivero et al., 2009). However, whether they perform this function independent of other factors and how they recruit γ-TuRC to MTOCs on a molecular level are not known.

The eight-subunit protein complex augmin mediates MT nucleation from preexisting MTs (Petry et al., 2013). Augmin targets γ-TuRC to spindle MTs based on the findings that knockdown of augmin subunits diminishes both MT density and γ-tubulin signals in the mitotic spindle (Goshima et al., 2007, 2008; Lawo et al., 2009; Uehara et al., 2009; Ho et al., 2011). To perform this function, augmin needs to bind to MTs and γ-TuRC. Out of the eight augmin subunits (denoted HAUS1–8 or H1–8), the augmin subunit HAUS8/Dgt4 is primarily responsible for binding to MTs (Wu et al., 2008; Hsia et al., 2014). In contrast, the C-terminal half of the augmin subunit HAUS6/Dgt6 binds to the adapter protein NEDD1, which in turn binds to γ-TuRC (Uehara et al., 2009). In addition, the N termini of HAUS3/Dgt3 and HAUS5/Dgt5 were identified as NEDD1-binding sites (Chen et al., 2017). Human augmin was recently shown to have a Y-shaped structure (Hsia et al., 2014), yet where the subunits and functional sites are located within the Y-shaped augmin complex and whether additional ones exist are not known. Besides augmin and γ-TuRC, the protein TPX2 is required for MT nucleation from a preexisting MT (Petry et al., 2013). TPX2 is a downstream target of RanGTP (Gruss et al., 2001) and has been suggested to activate γ-TuRC for branching MT nucleation (Alfaro-Aco et al., 2017).

Although augmin has been implicated in localizing γ-TuRC to spindle MTs, its molecular basis remains to be determined. Here, we show that augmin is a direct targeting factor for γ-TuRC to spindle MTs by reconstituting this activity in vitro. Furthermore, we dissect augmin's functional architecture, which explains how augmin performs this function.

Results

Establishing an assay for augmin activity in branching MT nucleation

To study augmin's function and mechanism, we reconstituted the *Xenopus laevis* augmin holocomplex by coexpressing all

[1]Department of Molecular Biology, Princeton University, Princeton, NJ; [2]Department of Biochemistry and Molecular Biophysics, Washington University School of Medicine, St. Louis, MO; [3]Department of Chemical and Biological Engineering, Princeton University, Princeton, NJ.

Correspondence to Sabine Petry: spetry@princeton.edu.

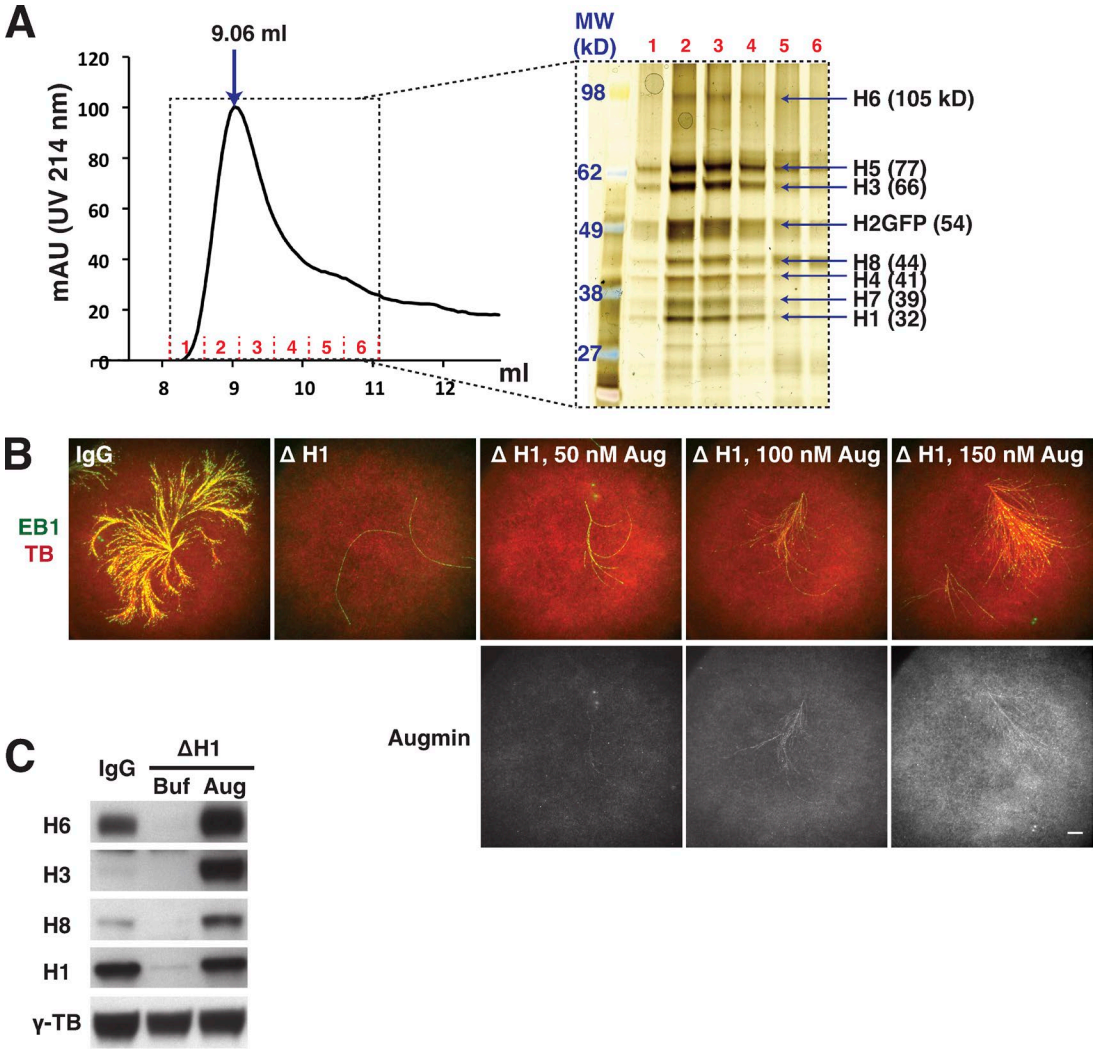

Figure 1. **Reconstituted *Xenopus* augmin recovers branching MT nucleation that was impaired by depletion of endogenous augmin in *Xenopus* egg extracts. (A)** The eight-subunit complex, augmin was stoichiometrically reconstituted in vitro, confirmed by size-exclusion chromatography using Superdex 200 increase 10/300 GL column. The calibrated void volume of the column is 8.73 ml. Fractions (1–6) were loaded to a SDS-PAGE gel (4–12% gradient), visualized by silver staining (right). **(B)** ID of endogenous augmin was performed using IgG as a control and anti-H1 antibody. Branching MT nucleation was activated by RanQ69L, in which Cy5-labeled tubulin and mCherry-labeled end-binding protein 1 (EB1-mCherry) highlight MTs and growing MT plus ends, respectively, pseudocolored in red and green. Bar, 10 µm. Recombinant augmin was added to the immunodepleted extract (Δ H1) at increasing concentrations, demonstrating that branching MT nucleation is restored in a concentration-dependent manner. Augmin localizes along the length of MTs, visualized by GFP in gray (bottom panel). Images were taken 35 min after sample preparation. **(C)** Anti-H1 antibody stoichiometrically depletes augmin subunits and add-back of 150 nM recombinant augmin to the H1-ID extract can be compared with the endogenous level (IgG). The fold changes for each subunit relative to the endogenous levels are depicted. These numbers are not absolute, because each antibody recognizes its antigen with different specificities.

eight subunits in SF9 insect cells and purifying the complex. Size-exclusion chromatography revealed that *Xenopus* augmin contains all eight subunits in equal stoichiometry, as previously reported for human augmin (Hsia et al., 2014; Fig. 1 A). To evaluate the functionality of recombinant augmin in physiological conditions, we established an activity assay consisting of several steps. First, we immunodepleted endogenous augmin from *Xenopus* egg extracts using custom-made antibodies against augmin subunits. Upon addition of constitutively active Ran (RanQ69L), branched MT networks formed in the control extract, whereas branching MT nucleation was no longer observed in the absence of augmin, as previously reported (Petry et al., 2013; Fig. 1 A). We selected the anti-HAUS1 (H1) antibody for these experiments because it completely depleted augmin while barely codepleting γ-TuRC. To test if our recombinant augmin was indeed active, we added it back to the augmin-depleted extract and assessed its activity via the branching reaction. Notably, recombinant augmin restored branching MT nucleation in a concentration-dependent manner and bound to MTs (Fig. 1 B and Video 1). Thus, reconstituted *Xenopus* augmin is active. We also note that the MT nucleation activity is reduced compared to the control reaction (Fig. S1), which could be due to a lack of posttranslational modifications and codepleted binding partners. In sum, this add-back system allowed us to directly study, for the first time, augmin's function while resolving individual MT nucleation events.

Augmin directly recruits γ-TuRC to MTs

Knowing that our recombinant augmin is active, we tested the key question whether augmin directly localizes γ-TuRC to MTs. We purified endogenous γ-TuRC from *Xenopus* egg extracts and verified its molecular content, size, and structure by mass spectrometry, sucrose gradient centrifugation, and negative-stain EM, respectively (Fig. S2, A and B). To first test whether augmin and γ-TuRC interact in solution, we incubated both purified complexes with each other and performed sucrose gradient sedimentation. As a result, augmin and γ-TuRC are marginally shifted and their fractions share some overlap compared with their individual sedimentation profiles (Fig. S2 A), consistent with previous findings in *Drosophila melanogaster* S2 extracts (Goshima et al., 2008) and our own investigations in *Xenopus* egg extracts (Fig. S2 C).

More importantly, can augmin directly target γ-TuRC to preexisting MTs? To test this, we performed MT cosedimentation assays. As expected from its minus-end–binding ability, γ-TuRC itself copelleted with Taxol-stabilized MTs at higher concentrations of 2 µM and 400 nM, but not at a lower concentration of 80 nM (Fig. 2, A and B). In contrast, in the presence of augmin, γ-TuRC was able to bind to MTs at this lower MT concentration of 80 nM and in an increased amount at 400 nM (Fig. 2, A and B), suggesting that γ-TuRC is recruited to additional binding sites on the MT via augmin. To assess where augmin targets γ-TuRC along the MT, we performed immunofluorescence (IF) of γ-TB on Cy5-labeled MTs incubated with either augmin or γ-TuRC or both (Fig. 2 C). In the absence of augmin, little γ-TuRC was detected on MTs (Fig. 2 C). However, when added together, both augmin and γ-TuRC specifically localized along the whole length of MTs (Fig. 2 C). Quantification of the γ-TuRC signal (normalized to the MT signal to account for MT bundling by augmin) revealed that addition of augmin significantly increases γ-TuRC localization to MTs (Fig. 2 D). Although augmin induced MT bundling, single augmin-bound MTs onto which γ-TuRC was recruited were also detected (Fig. S2 D). Thus, we reconstituted γ-TuRC localization along the length of MTs via augmin in vitro and thereby uncovered augmin as a direct targeting factor for γ-TuRC.

Because addition of the other essential branching factor TPX2 to *Xenopus* egg extracts induces the formation of branched fanlike structures (Petry et al., 2013), we tested whether recombinant augmin can promote MT nucleation from γ-TuRC in addition to being its localizer. When augmin is added to *Xenopus* egg extracts, it does not increase the number of MTs formed in extract (Fig. S3 A). This is in contrast to TPX2, which stimulates branching MT nucleation in extract (Petry et al., 2013; Alfaro-Aco et al., 2017). Moreover, augmin does not enhance the nucleation capacity of purified γ-TuRC in vitro (Fig. S3 B). These results further support that augmin's function is to localize γ-TuRC along the length of MTs.

Analysis of augmin's subunit architecture reveals two subcomplexes

To study how augmin targets γ-TuRC to MTs, we sought to reveal how the eight subunits are arranged within the augmin holocomplex and performed two complementary interaction analyses. First, augmin antibodies were used to identify interacting augmin subunits by immunoprecipitation (IP) followed by Western blot (Fig. 3 A). Furthermore, these IP samples were labeled with different isobaric tandem mass tags and analyzed by quantitative liquid chromatography tandem mass spectrometry (Fig. 3 B), followed by hierarchical clustering to reveal how augmin is assembled (Fig. 3 C). The subunit H8 was shown to directly interact with H6 (Hsia et al., 2014), and this interaction was taken into account for clustering. Based on the resulting dendrogram, we propose two subcomplexes: one subcomplex includes H6, H7, and H8, whereas another one contains H1, H3, H4, and H5 (Fig. 3 D). H2 could have a role in connecting the two subcomplexes, or it could be peripheral (Fig. 3 D). Independently, we used our recombinant augmin expression system to probe direct interactions between two augmin subunits by in vitro pull-down assays (Fig. S4). Each subunit was tested to bind to each of the other subunits (Fig. S4) and unidirectional and reciprocal interactions are depicted in a summary table (Fig. 3 E). These in vitro interaction data were combined with the IP-based hierarchical clustering data to derive the following model for augmin assembly (Fig. 3 F). Reciprocal interactions exist between three subunit pairs, namely, H1/H4, H3/H5, and H6/H8. H6 appears to be the core of the complex because it interacts with five subunits (H1, H2, H4, H7, and H8). As a result, our data suggest that augmin might be assembled via several subcomplexes.

All eight augmin subunits are required for branching MT nucleation

To test the predicted augmin assembly model, we attempted to coexpress and purify different combinations of subunits. Besides the augmin holocomplex, which contains all subunits, we generated an augmin octamer(H6ΔC) that contains all eight subunits, only that its H6 lacks the C-terminal half, which is known to interact with NEDD1 (Uehara et al., 2009; Hsia et al., 2014; Fig. 4, A and B). We were unable to reconstitute the trimer consisting of H6, H7 and H8 subunits, even when using the more soluble form of H6 lacking its C-terminal half (H6ΔC). Instead, the subunit H2 was required to reconstitute H6ΔC, H8, and H7 into a soluble tetramer (tetramer II [T-II]), consisting of the same subunits as the previously denoted T-II made from human augmin (Hsia et al., 2014). The remaining four subunits (H1/4/3/5) associated as a stable complex, which we denote as T-III (Fig. 4, A and B). The previously reported T-I of human augmin, consisting of subunits H6ΔC, H8, H1, and H4, could not be formed with our *Xenopus* subunits (Hsia et al., 2014). Each tetramer could not be broken down into smaller complexes, except for one dimer consisting of H1 and H4 that was soluble. Also, adding more subunits to each tetramer for coexpression and purification did not result in any monodisperse complexes. This suggests that both tetramers are unique and stable subcomplexes that make up the augmin holocomplex.

Next, we wanted to assess the functions of both tetramers compared with the augmin holocomplex and octamer(H6ΔC). For this purpose, each complex was added to the augmin-depleted extract and tested for their ability to promote branching MT nucleation. Both the augmin holocomplex and octamer(H6ΔC) restored branching MT nucleation, although the octamer(H6ΔC) displayed a reduced level of activity caused by the absence of H6's

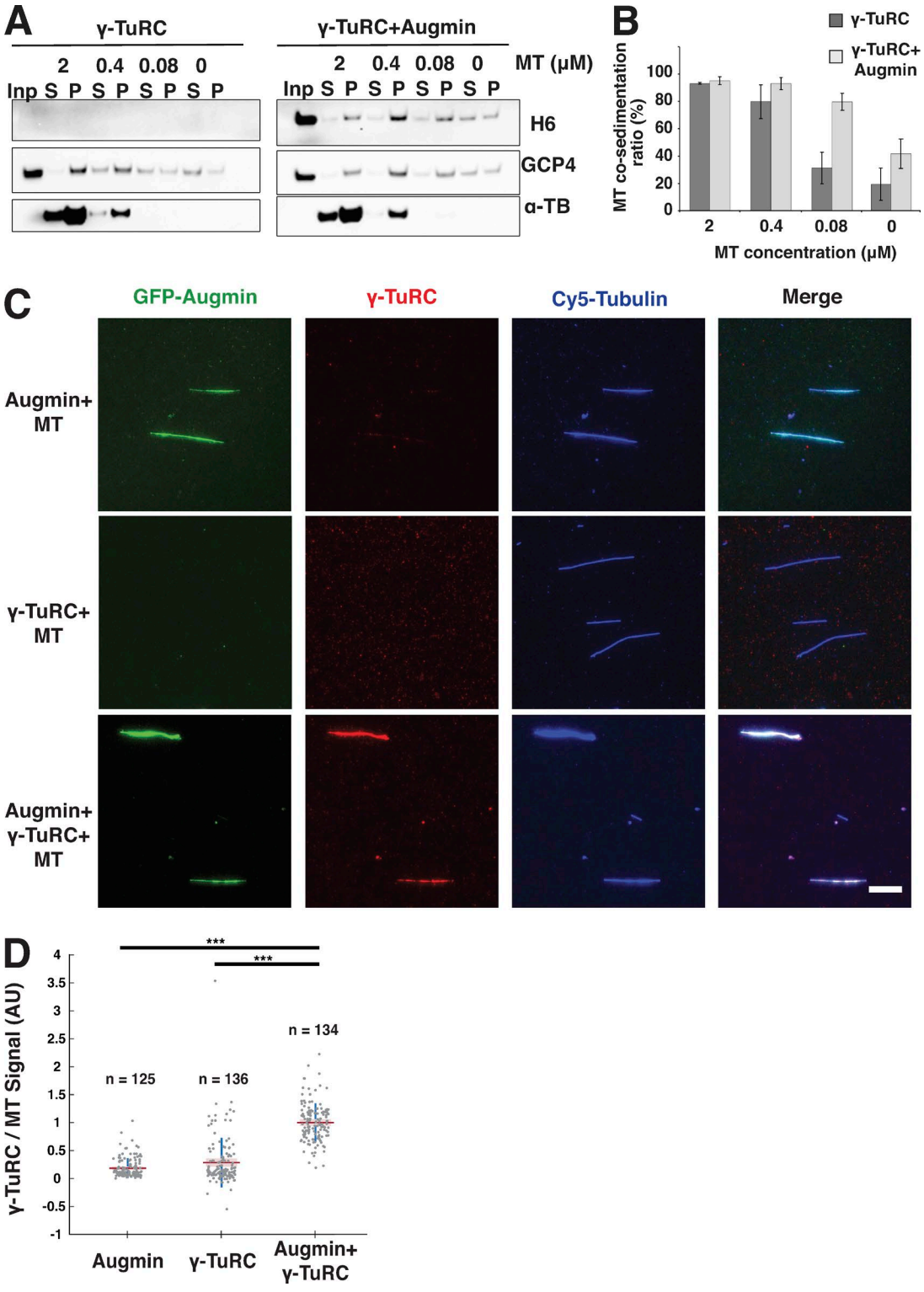

Figure 2. **Augmin directly recruits γ-TuRC to MTs. (A)** MT cosedimentation assays were performed with γ-TuRC and γ-TuRC plus augmin at different concentrations of MTs (2, 0.4, 0.08, and 0 µM), demonstrating augmin-dependent recruitment of γ-TuRC to MTs. **(B)** Quantification of MT cosedimentation assay results. MT cosedimentation ratios of γ-TuRC without and with augmin were calculated for each MT concentration using averaged signals of GCP4 from Western blots using two independent experiments. An error bar denotes ± standard deviation across replicates. **(C)** IF of γ-tubulin (red, 568 channel) on prepolymerized Cy5-MTs in the absence of γ-TuRC (top panel), the absence of GFP-Augmin (middle panel), or the presence of both (bottom panel). Bar, 10 µm. **(D)** Boxplot of γ-TuRC signal relative to MT signal. Each dot represents a single MT, pink boxes denote ± 1 standard deviation, blue lines show the 95% confidence interval, and red bars show the mean. Triple asterisks (***) denote a p-value below 0.0001. The numbers of MTs (n) were obtained from three independent experiments.

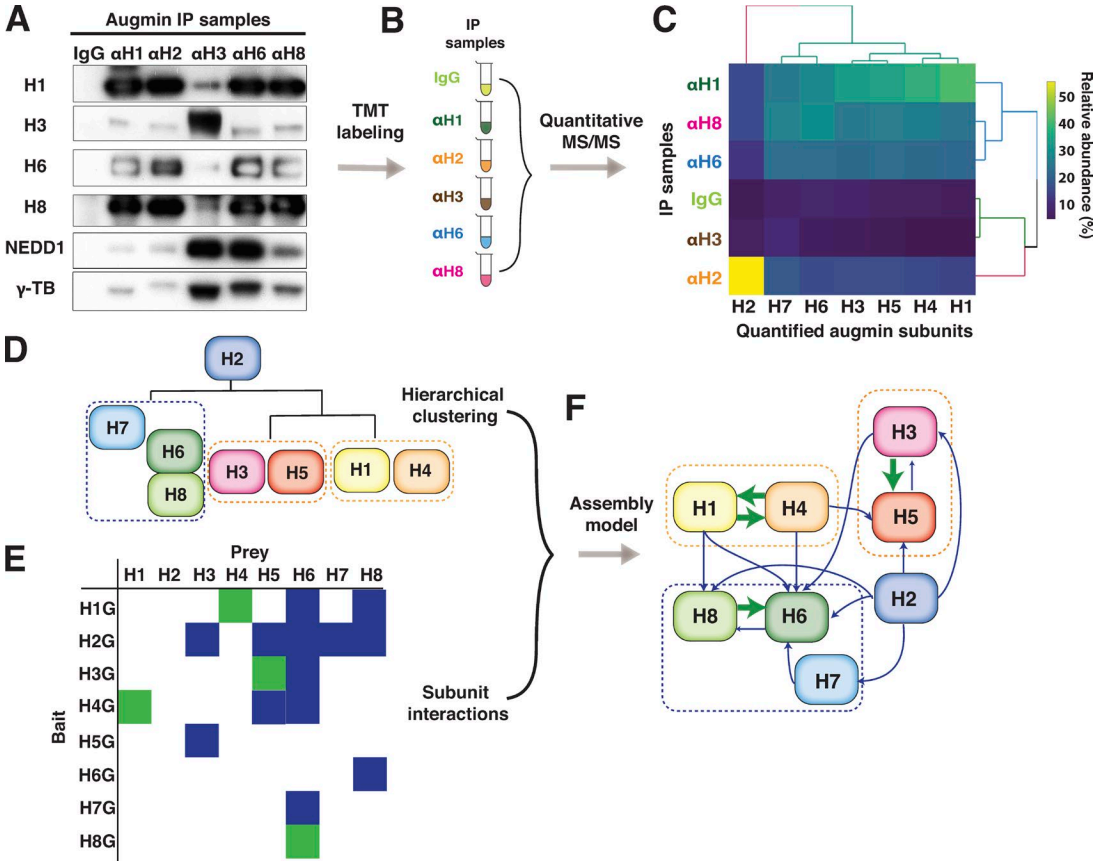

Figure 3. ***Xenopus* augmin subunit assembly and interactions. (A)** Augmin IP was performed with antibodies IgG, anti-H1 [αH1], αH2, αH3, αH6, and αH8, and checked by Western blot. **(B)** Proteins in IP samples were identified and quantified by SixplexTMT labeling and liquid chromatography tandem mass spectrometry analyses. **(C)** Quantified peptides were normalized, providing relative intensities of augmin subunits (H1–H7) in each IP sample. Data were visualized by a heatmap with hierarchical clustering, generated using the heapmaply package of R. **(D)** Hierarchical clustering dendrograms were drawn to include H8 that directly binds to H6, showing the assembly of all augmin subunits. **(E)** In vitro pull-down assays were performed to identify all interactions between augmin subunits (Fig. S3). All interactions are summarized; a green square stands for a strong interaction and blue for a weak. Strep-GFP tagged subunits were used as bait and the other seven subunits as prey. **(F)** All data resulted in a model of augmin assembly in which the direction of arrows point from bait to prey subunits.

C terminus (Fig. 4 C and Video 2). However, neither T-II nor T-III elicited branching nucleation after the depletion of endogenous augmin (Fig. 4 C and Video 2).

T-II and T–III target γ-TuRC to MTs via complementary activities

To assess why T-II and T-III independently cannot replace endogenous augmin and to determine their function, we tested the ability of each complex to bind MTs. Augmin T-II, similar to holocomplex and octamer(H6ΔC), binds to and bundles guanylyl-(α,β)-methylene-diphosphonate (GMPCPP)–stabilized MTs (Fig. 5 A). In contrast, T-III was not able to bind to MTs. These results are consistent with the finding that H8 within T-II of human augmin is mainly responsible for MT binding (Hsia et al., 2014). To act as a recruiting factor, augmin must also bind to γ-TuRC. To test this, we performed IP experiments using anti-GFP antibodies specific for GFP-tagged recombinant augmin complexes that were added back to augmin-depleted *Xenopus* egg extracts. Our results demonstrate that γ-TuRC interacts with the augmin holocomplex and, unexpectedly, with the octamer(H6ΔC) in the extract (Fig. S5 A). Thus, in contrast to previous work (Uehara et al., 2009), H6's C-terminal lacking in the octamer(H6ΔC) is not required for γ-TuRC binding (Fig. S5 A), implying other γ-TuRC binding sites must exist. Interestingly, an interaction between γ-TuRC and T-III (H1/4/3/5) was detected (Fig. S5 A), thus uncovering T-III as a novel γ-TuRC–binding subcomplex of augmin. Importantly, this interaction pattern in the extract is in agreement with pull-down results performed in vitro with purified components (Fig. 5 B). Finally, we analyzed which components of T-III are responsible for γ-TuRC binding. Neither the individual subunits H3 and H5 nor the dimer H1/4 were able to bind to γ-TuRC (Fig. S5 B). Only the complete T-III binds to γ-TuRC, suggesting that the folded tetramer provides the functional binding site. In light of these findings, we tested whether T-II is sufficient to recruit γ-TuRC along the MT length with purified components. As expected, T-II was not able to perform this function, as it lacks the γ-TuRC–binding modules (Fig. S5 C). In summary, we identified two functionally distinct subcomplexes: T-III (H1/4/3/5) mediates γ-TuRC binding, and T-II (H6ΔC/8/2/7) binds to MTs. Both complementary activities (MT and γ-TuRC binding) need to be present in augmin for branching MT nucleation, suggesting that augmin directly bridges MTs and γ-TuRC.

To investigate the structure of the newly identified functional parts, we visualized augmin complexes by negative-stain EM. 2D class averages reveal that *Xenopus* augmin has a Y shape

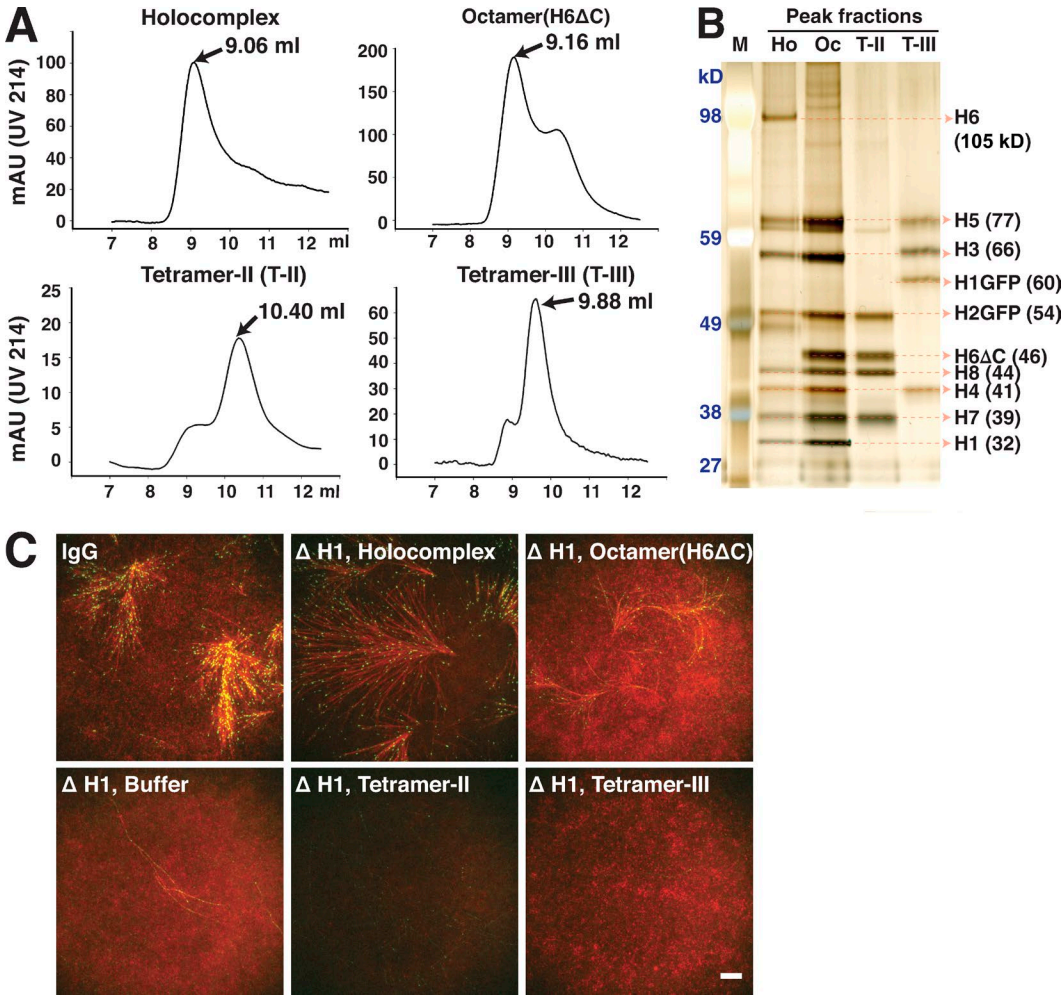

Figure 4. **Augmin complexes exhibit varying activities in branching MT nucleation. (A)** Four augmin complexes were generated based on the model of augmin assembly and confirmed by size-exclusion chromatography using a Superdex 200 increase 10/300 GL column. The peak elution volume of each complex was determined. **(B)** Peak fractions were analyzed by a SDS-PAGE gel (silver staining), showing the components of each complex and stoichiometric complex formation. **(C)** Augmin complexes (150 nM) were added back to the augmin-depleted extract (Δ H1), and their activities were examined by branching MT nucleation assays. EB1 is shown in green and MTs in red. Bar, 10 µm. Images were taken 35 min after sample preparation. IgG is the control extract without augmin depletion.

similar to human augmin (Hsia et al., 2014; Fig. 5 C and Fig. S6 A). Interestingly, our newly identified T-III has a rod shape, which roughly matches the stalk of augmin's Y shape in dimensions and appearance (Fig. 5 C and Fig. S6 B). We were unable to obtain 2D class averages of the T-II subcomplex with a defined shape, suggesting that T-II is relatively flexible by itself and will only adopt a V-shape conformation when bound to the other tetramer (Fig. 5 C). Finally, we visualized augmin bound to MTs by negative-stain EM, in which the T-III stalk points away from the MT in a perpendicular manner (Figs. 5 D and S5 D). Altogether, this shows the functional architecture of augmin, in which T-II interacts with the MT lattice, whereas the complete T-III protrudes out from the MT to interact with γ-TuRC (Fig. 5 E).

Discussion

In summary, our data lead to a model (Fig. 5 E) in which augmin binds to MTs via T-II and recruits γ-TuRC predominantly via T-III. Our data suggest H6's C terminus is dispensable for γ-TuRC binding in vitro. To compare the exact contribution to γ-TuRC binding between the originally proposed C terminus of H6 and the newly identified T-III, it will be necessary to quantitatively compare their binding affinities to γ-TuRC. Although the complete T-III is sufficient to bind γ-TuRC, H6 may be located in the vicinity of T-III where it can also bind to γ-TuRC via NEDD1 (Fig. 5 E). This is in agreement with recent work in *D. melanogaster* where Dgt3 (H3), Dgt5 (H5), and Dgt6 (H6) were proposed to interact with Dgp71WD (NEDD1; Chen et al., 2017). It will be interesting to see whether the stalk-like T-III that directly binds to γ-TuRC could be a common structural feature of other γ-TuRC targeting factors.

In this study, we provide an interaction model of augmin's subunits and place them into functional tetramers. Because each tetramer cannot be broken down into smaller units (except for the H1–H4 dimer), the tetramers assume an elongated structure, and each subunit seems to consist mostly of α-helices by secondary structure prediction (Drozdetskiy et al., 2015), it is likely that each tetramer's four subunits fold into a helical

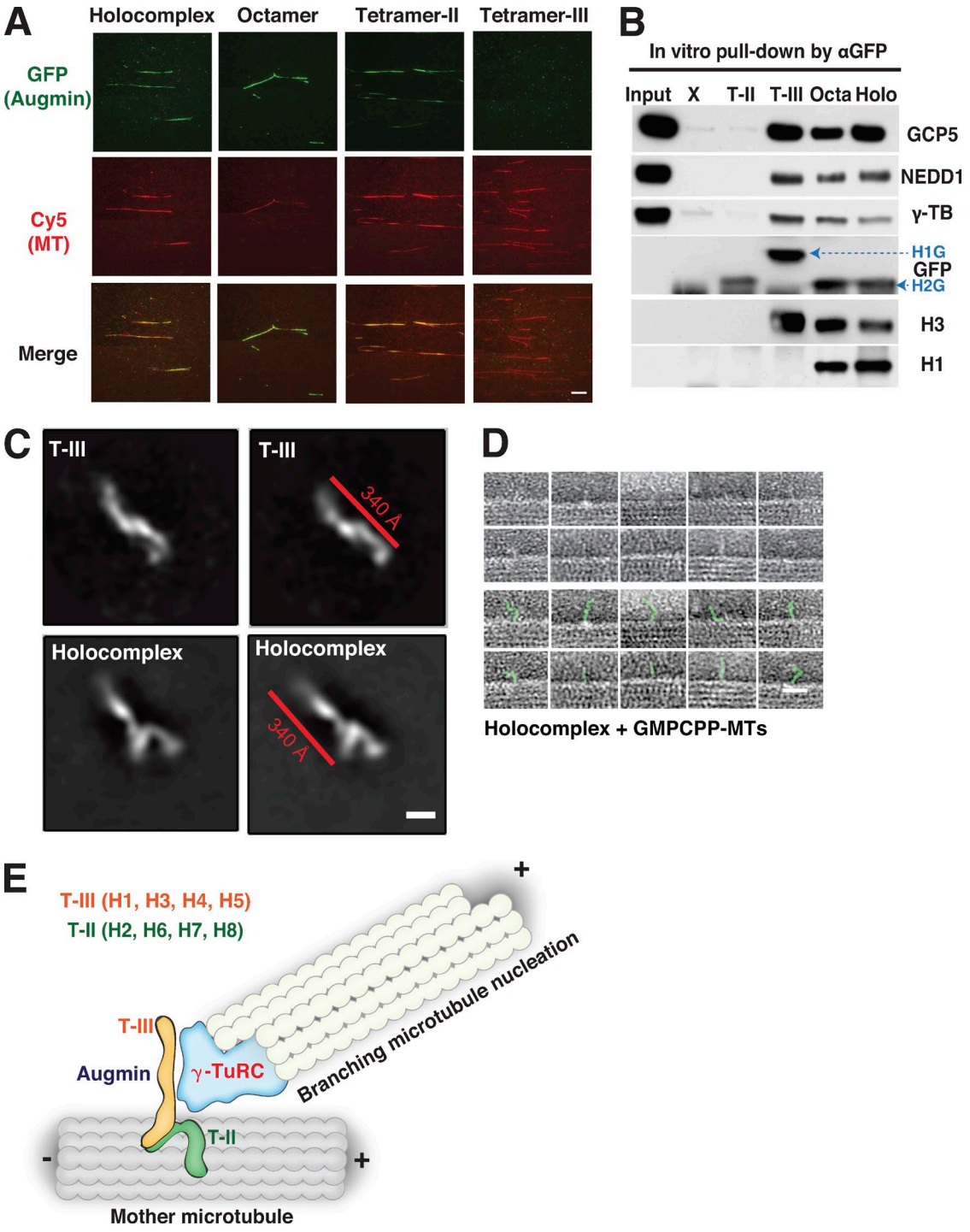

Figure 5. **Augmin interacts both with γ-TuRC and MTs via complementary subcomplexes. (A)** 150 nM augmin complexes were mixed with GMPCPP-MT seeds and visualized by TIRF microscopy. Augmin is displayed in green and MTs in red. Bar, 10 µm. **(B)** In vitro pull-down assays were performed using purified γ-TuRC and four augmin complexes and analyzed by Western blots. Because the GFP-tag is common among the four complexes, anti-GFP antibody (αGFP) was used for pull-down assays. The results demonstrate that augmin holocomplex, octamer(H6ΔC), and T-III directly interact with γ-TuRC; however, T-II does not. Input is the 1:5 dilution of purified γ-TuRC sample used for pull-down assays. X denotes negative control in which no augmin is used as bait. **(C)** Negative-stain analysis of augmin. 2D class averages of augmin complexes generated by Relion-2. Two representative class averages for both holocomplex (holo) and T-III are shown. Bar, 10 nm. Each class average for the holo and T-III contains ~1,000 and 2,000 raw particle images, respectively. The class averages appear fuzzy at the distal ends, suggesting some level of flexibility for the complex. **(D)** Representative images of augmin holocomplex on GMPCPP-MTs. Bar, 20 nm. **(E)** A model for augmin-mediated localization of γ-TuRC to MT for branching MT nucleation.

coiled-coil structure (Fig. 5 C). An important next step will be to determine the location of each subunit within the holocomplex and ideally to obtain a high-resolution structure at the atomic level of augmin.

Interestingly, branching of actin filaments is generated with a fixed angle of 70 degrees because of the stable structure of the Arp2/3 complex (Mullins et al., 1998; Robinson et al., 2001). In contrast, branching MT nucleation occurs mostly parallel and with a range of shallow angles (Petry et al., 2013). Our structural data can rationalize this behavior, because augmin mostly binds to MTs in a perpendicular manner but still adopts various conformations around that angle (Figs. 5 D and S5 D). In the future, a 2D class average model of augmin bound to a MT can be obtained by collecting a myriad of particles.

We quantified MT nucleation kinetics in IgG and holocomplex add-back conditions (Fig. 1 B) by tracking EB1 comets (Fig. S1), which revealed two key differences. First, MT nucleation in the augmin add-back condition was delayed compared with the IgG control. Second, the total number of MTs was less upon augmin add back compared with the IgG control. Several explanations could account for these differences. It is possible that recombinant augmin might need to be activated in extracts, and extra time for posttranslational modifications or binding to endogenous partners like γ-TuRC is required after add back. During immunodepletion (ID), augmin-binding partners could get codepleted, which is common in this assay. In fact, coimmunoprecipitated proteins were identified using quantitative mass spectrometry (Fig. 3 C), including γ-TuRC components, and the absence of those proteins could prevent total recovery of MT nucleation after add back. It will be necessary to thoroughly investigate the function of augmin binding partners and their role in making branching MT nucleation more efficient.

It has been reported that recombinant human augmin independently produces asters and enhances Ran aster number in a dose-dependent manner in *Xenopus* egg extracts (Hsia et al., 2014). Instead, by using branching MT nucleation and total internal reflection fluorescence (TIRF) microscopy, we resolve individual, augmin-dependent MT nucleation events and show that *Xenopus* augmin does not change the number of MTs. Furthermore, we show that purified augmin does not activate purified γ-TuRC in vitro.

Interestingly, augmin seems to entirely decorate MTs within the branched fan-like structures (Fig. 1 B), yet new MTs only originate from discrete locations and with a certain delay along the MT lattice. Combined with our observation that augmin addition to γ-TuRC does not cause increased MT nucleation (Fig. S3 B), this suggests that the augmin–γ-TuRC interaction is not sufficient to nucleate a new MT from a preexisting MT. Additional factors may be required for MT nucleation from a preexisting MT. The missing piece could be TPX2, which is also essential for branching MT nucleation (Petry et al., 2013) and which was recently proposed to act as a γ-TuRC activator (Petry et al., 2013; Alfaro-Aco et al., 2017). Furthermore, γ-TuRC requires XMAP215 to synergistically nucleate MTs (Thawani et al., 2018). It will be critical to fully reconstitute branching MT nucleation in vitro to identify all factors involved along with their role and to establish the molecular mechanism of branching MT nucleation.

Materials and methods

Protein expression and purification

Xenopus augmin genes were cloned into pFastBac vectors for the use of Bac-to-Bac baculovirus expression system (Invitrogen), individually with and without N-terminal Streptag conjugated with GFP. Additionally, H3, H6ΔC (amino acids 1–430), and H6 (amino acids 1–978) genes were cloned with N-terminal ZZ tag (ZZ-H3, ZZ-H6, and ZZ-H6dC; Nilsson et al., 1987; Reck-Peterson et al., 2006) and H1 and H2 genes with C-terminal GFP-Histag (H1CG-His and H2CG-His) for the sequential affinity purifications.

Recombinant baculoviruses were amplified to reachviral titers of 10^9 pfu/ml. For the expression of augmin complexes, 1–2 liters of SF9 cells (1.5–2.0 × 10^6/ml) were infected with each baculovirus at a MOI of 1–3, which were collected after 72 h. The following baculovirus combinations were used for each augmin complex: holocomplex with ZZ-H6, H2CG-His, and the remaining six subunits without tag; octamer(H6ΔC) with ZZ-H6ΔC, H2CG-His, and the rest of six subunits without tag; T-II with ZZ-H6ΔC, H2CG-His, H7, and H8; and T-III with ZZ-H3, H1CG-His, H4, and H5.

Harvested insect cells were resuspended with lysis buffer containing 20 mM Tris, pH 7.4, 150 mM NaCl, 3 mM β-mercaptoethanol, 0.05% (vol/vol) Tween-20, and Complete EDTA-free protease inhibitor (Roche) and lysed by EmulsiFlex (Avestin), followed by centrifugation at 80,000 *g* for 30 min at 4°C. Cleared lysates were mixed with 1–2 ml of IgG-Sepharose (GE Healthcare) slurry for 2 h using rotator at 4°C. IgG beads were collected via a chromatography column (Econo-Column; Bio-Rad) and then washed with 20 times of bed volume of TBS-T (Tris-buffered saline, pH 7.4, with 0.1% [vol/vol] Tween 20). Washed IgG beads were mixed with 3C protease cleavage buffer (20 mM Tris, pH 7.4, 150 mM NaCl, 3 mM β-mercaptoethanol, 10% [vol/vol] glycerol, and 100–200 µg of GST-HRV3C protease). Augmin complexes were eluted from IgG beads by protease cleavage overnight at 4°C. On the following day, 3C protease was removed by GSTrap column (GE Healthcare). 1 ml Ni-NTA agarose slurry (QIAGEN) was added to the flow-through fraction of GSTrap column and incubated for 1 h at 4°C. Ni-NTA beads were collected with Poly-Prep chromatography columns (Bio-Rad) and washed with 10 ml of Ni-NTA wash buffer (20 mM sodium phosphate, pH 7.4, 200 mM NaCl, and 20 mM imidazole). Augmin complexes were eluted by Ni-NTA elution buffer (Ni-NTA wash buffer with 300 mM imidazole), followed by gel filtration chromatography using Superdex 200 increase 10/300 GL (GE Healthcare) column equilibrated with TBS, pH 7.4, to confirm complex formations or by dialysis overnight at 4°C with CSF-XB buffer containing 10 mM Hepes, pH 7.7, 100 mM KCl, 1 mM $MgCl_2$, 5 mM EGTA, and 10% (wt/vol) sucrose. Augmin complexes in CSF-XB buffer were flash-frozen with liquid nitrogen and stored at −80°C for functional assays. The void volume of the gel filtration column (8.73 ml) was determined by running 2 mg/ml blue dextran 2000 (GE Healthcare). Protein concentrations were measured at UV 280 nm by NanoDrop (Thermo Fisher Scientific) using the extinction coefficient corresponding to each protein complex.

Preparation of augmin antibodies

Rabbit polyclonal antisera against *Xenopus* H1 (1–861 bp), H2 (1–669 bp), H3 (1–1794 bp), H6 (1873–2973 bp), and H8 (1–1,118

bp) were generated by custom antibody production service (GenScript). For antibody purification from antisera, antigens were conjugated to Affi-gel 10 or 15 (Bio-Rad) overnight at 4°C in coupling buffers according to the product instruction. On the following day, the antigen-coupled beads were washed with PBS, pH 7.4, and 0.1 M glycine, pH 2.5, followed by equilibration with PBS. Then, antisera were diluted in PBS (1:4) and incubated with antigen-coupled beads for 2 h at 4°C, followed by washing with PBS with 0.5 M NaCl. The beads were washed again with PBS to remove salts. Antibodies were eluted with 0.1 M glycine, pH 2.5, and the buffer quickly neutralized with 1 M Hepes, pH 7.7 (1:10 ratio).

Branching MT nucleation assay

Cytostatic factor (CSF)–arrested *Xenopus* egg extracts were prepared as described (Hannak and Heald, 2006). For branching MT nucleation assay, 6.5 µl of the extract was mixed with 1.5 µl of 1 µM augmin complexes (or CSF-XB buffer), 0.5 µl of 10 mM vanadate, 0.5 µl of 200 µM RanQ69L, 0.5 µl of 1 µM mCherry-EB1, and 0.5 µl of 2 µM Cy5-labeled porcine tubulin in 10 µl reaction volume. The extract mixture was introduced into the flow cell as described previously (King and Petry, 2016). Images were collected on a Nikon TiE microscope using a 100× 1.49 NA oil-immersion TIRF objective and three laser channels(488, 561, and 641 nm). Images were acquired on Nikon elements software with an Andor Zyla sCMOS camera. Images were collected every 2 s for 20–30 min.

ID of endogenous augmin

150 µl Dynabeads Protein A (Life Technologies) were equilibrated with TBS-T and coupled with 35 µg of each antibody overnight at 4°C. Antibody-conjugated beads were washed three times with 150 µl TBS-T and two times with 150 µl CSF-XB. The beads were retrieved by magnetic separation rack and split into two tubes, which were sequentially mixed with 65 µl CSF extracts and placed on ice for 45 min for each round. Immunodepleted extracts were retrieved and transferred to another tube on ice.

IP and protein quantification by mass spectrometry

After carrying out ID, beads were retrieved from the immunodepleted extracts and washed three times with 150 µl TBS-T. Immunoprecipitated samples were eluted from beads with 0.1 M glycine, pH 2.5. Proteins in the eluates were identified and quantified by the Thermo Fisher Scientific Center for Multiplexed Proteomics at Harvard Medical School (Boston, MA) after sixplex isobaric tandem mass tag (Thermo Fisher Scientific) labeling. Quantified peptides were normalized to the summed signal across all samples, which were used to generate the heatmap and hierarchical clustering using the "heatmaply" package of R.

Western blot

After running SDS-PAGE gels with immunodepleted extracts or IP samples, proteins were transferred to nitrocellulose membranes, which were incubated with blocking buffer containing TBS-T and 10% (wt/vol) fat-free dry milk for 30 min, followed by incubation with primary antibodies that were used for ID and IP in blocking buffer for 1 h at RT or 4°C overnight. Membranes were washed three times for 15 min each with blocking buffer and then incubated with HRP-conjugated secondary anti–mouse or anti–rabbit IgG antibodies (GE Healthcare) in blocking buffer (1:3,000 dilution) for 1 h at RT or 4°C overnight. Membranes were washed three times for 15 min each with TBS-T. ECL solutions were added to the membranes for chemiluminescence detection. For the detection of γ-TuRC components, the following commercial antibodies were used: anti-NEDD1 antibody (ab57336; Abcam), anti–γ-TB antibody (T6557; Sigma), anti-GCP4 antibody (sc-271876; Santa Cruz Biotechnology), and anti-GCP5 antibody (sc-365837; Santa Cruz Biotechnology).

In vitro pull-down assays for augmin subunit interactions

Each augmin subunit with Strep-GFP tag was expressed alone and coexpressed with each of the other seven subunits by baculovirus coinfection to 50 ml of insect cells ($1.5–2.0 \times 10^6$). Cells were harvested by centrifugation at 3,000 *g* for 20 min, followed by resuspension with the lysis buffer described above. Cells were lysed by sonication, and lysates were cleared by centrifugation at 17,000 *g* for 30 min. 100 µl Strep-Tactin (IBA) slurry was added to each supernatant and mixed with rotator for 2 h at 4°C. Beads were collected by centrifugation at 4,000 *g* for 3 min, followed by three washes with 10 ml TBS. Samples were eluted by boiling with SDS-PAGE sample buffer and loaded to a SDS-PAGE gel (4–12% polyacrylamide gradient).

Add back of augmin complexes to the immunodepleted extract and IP for the interaction of γ-TuRC and augmin

Augmin complexes (150 nM) were added back to the immunodepleted extract, followed by branching MT nucleation assays as described above. For IP experiments, anti-GFP antibody (ab290; Abcam)–conjugated Dynabeads were prepared as for ID experiments. Augmin complexes (150 nM) were added to the ID extract (15 µl) to make up 20 µl of samples and incubated for 30 min on ice. Anti-GFP antibody conjugated Dynabeads (20 µl) were retrieved and mixed with the extract samples. The extract sample and beads were mixed for 1 h by rotation at 4°C. The beads were collected from the extract sample and washed three times with 150 µl TBS-T. Samples were eluted by boiling with SDS-PAGE sample buffer, followed by Western blot.

In vitro MT binding assay

20 µM bovine tubulin was mixed with 2 µM biotinylated porcine tubulin, 2 µM Cy5-tubulin, and 1 mM GMPCPP in BRB80 buffer (80 mM K-Pipes, pH 6.8, 1 mM EGTA, and 1 mM $MgCl_2$) on ice. The tubulin mixture was incubated at 37°C for 1 h. The polymerized GMPCPP MT seeds were diluted with BRB80 (1:400) and mixed with 150 nM augmin complexes. Dimethyldichlorosilane-treated coverslips were used to make flow cells. 0.1 mg/ml anti-biotin antibody was applied to the coverslip and unattached antibodies were washed out with 50 µl BRB80, followed by blocking with 1 mg/ml kappa-casein. After washing with 50 µl BRB80, MT/augmin mixtures were attached to the coverslip via anti-biotin antibodies. After a final wash with BRB80 supplemented with oxygen scavenging system (Trolox, PCA, and PCD; Aitken et al., 2008), the sample was imaged.

Purification of endogenous γ-TuRC from *Xenopus* egg extracts

10 ml of *Xenopus* egg extract was diluted with 5 vol of CSF-XB buffer supplemented with 1 mM GTP and Complete EDTA-free protease inhibitor (Roche), followed by spinning at 3,000 *g* for 10 min at 4°C to pellet any large particles. The supernatant was further diluted twofold with CSF-XB buffer containing 1 mM GTP and filtered through a 22-µM filter. γ-TuRC was precipitated from the filtered extract by addition of 6.5% (wt/vol) polyethylene glycol 8000 and incubated on ice for 30 min. After centrifugation for 20 min at 17,500 *g* at 4°C, the polyethylene glycol pellet was resuspended in 20 ml CSF-XB buffer with 0.05% NP-40. The resuspended pellet was centrifuged at 136,000 *g* at 4°C for 7 min. The supernatant was then precleared with recombinant protein A Sepharose beads (GE Healthcare) for 20 min at 4°C. The beads were removed, 1 ml γ-tubulin antibody (1 mg/ml) was added to the sample, and the sample was incubated at 4°C for 2 h with rotation. After this, 1 ml of washed recombinant Protein A Sepharose beads was incubated with the sample on the rotator for 2 h. The sample was then centrifuged at 500 *g* for 5 min and the flow-through removed. The beads containing bound γ-TuRC were washed twice with 10 ml CSF-XB buffer with 0.05% NP-40 and poured onto a column. The beads were then washed with CSF-XB buffer containing 250 mM KCl (30 ml), with CSF-XB buffer with 1 mM ATP to 10 ml remove heat-shock proteins, and finally with 10 ml of CSF-XB buffer. 1 ml γ-tubulin peptide (residues 412–451) at 0.4 mg/ml in CSF-XB buffer was applied to the column and allowed to incubate overnight. The following day, additional CSF-XB buffer was added to the column and fractions 1–5 (0.5 ml each) were collected. All fractions contained γ-TuRC, with fractions 1–3 having the highest concentration of γ-TuRC.

Sucrose gradient centrifugation

Sucrose was dissolved in CSF-XB buffer (without sucrose) to prepare light and heavy solutions (10–50% or 15–45% [wt/vol]). Continuous sucrose gradient was made by mixing the two solutions using Gradient Master (Biocomp). After loading samples, differential centrifugation was performed using TLS-55 rotor (Beckman Coulter) at 200,000 *g* for 4 h at 4°C. Samples were fractionated and loaded on SDS-PAGE gels, followed by Western blot analyses to determine γ-TuRC containing fractions.

MT nucleation assay with purified γ-TuRC

Purified bovine brain α, β-tubulin was purchased (PurSolutions). γ-TuRC obtained after sucrose gradient fractionation was concentrated and exchanged into BRB80 buffer using an Amicon Ultra-4 ml 10,000 NMWL centrifugal filter units. Before use in the assay, unlabeled α, β-tubulin + 10% Alexa Fluor 568–labeled porcine brain tubulin, BRB80 buffer and 1.5 mM GTP was combined and clarified by centrifugation at 80,000 rpm (TLA100.1 rotor; Beckman Coulter) for 20 min at 2°C. A sample of the clarified tubulin mixture was reserved for confirmation of final tubulin concentration in the reaction. The final concentration used in the nucleation reactions was similar for each experiment and ranged from 10 µM to 12 µM. The clarified tubulin mixture was combined with γ-TuRC with or without recombinant augmin at described concentrations to a final volume of 20 µl. The solution was mixed on ice, allowed to rest for 2 min, and then incubated at 37°C for 5 min. The nucleation mixture was then diluted with 80 µl warm BRB80, terminated with the addition of 100 µl of 2% glutaraldehyde in BRB80 buffer (for final glutaraldehyde concentration of 1%), and left at RT for 5 min. The samples were then diluted 10-fold in BRB80 buffer, layered on top of 5 ml cushion of 20% (vol/vol) glycerol in BRB80 buffer prepared in a 15 ml Corex tube fitted with a custom insert to support a round poly-lysine–coated coverslip. The sample was centrifuged for 45 min at 25,000 *g* in an HB-6 rotor at 4°C. After centrifugation, the cushion was removed and ice-cold methanol was added to the tube. The coverslip was mounted in Prolong Diamond and imaged with TIRF microscopy on Nikon TiE microscope using 100× 1.49 NA oil immersion TIRF objective. The images were acquired with Andor Zyla sCMOS camera. All images from each experiment were taken with the same TIRF angle and the same laser exposure during the same imaging session. At least 20 random fields of equal size were imaged for each sample, and representative images are shown.

Negative-stain EM and data processing

10–50 nM augmin complexes (5 µl) were introduced onto carbon EM grids and stained with 2% uranyl acetate. The negative-stain data for holocomplex, T-II, and T-III were collected using a FEI Tecnai F20 Twin transmission electron microscope operating at 120 keV at a nominal magnification of 50,000 with a defocus ranging from −2 to −3 µm. A total of ∼200 images for each sample were automatically recorded on a Gatan 4k × 4k-pixel charge-coupled-device camera using the LEGINON data collection software (Suloway et al., 2005). The calibrated pixel size of the recorded image is 2.1 Å.

The contrast transfer function was estimated using CTFFIND3 program within the APPION processing environment (Mindell and Grigorieff, 2003; Lander et al., 2009). The particles were automatically picked from the raw micrographs using a template-based method in Gautomatch program (http://www.mrc-lmb.cam.ac.uk/kzhang/Gautomatch/). Particle images stacks were generated by Relion-2 program featuring GPU acceleration (Kimanius et al., 2016). The reference-free 2D classification of the particle image stack was also performed in Relion-2 using 50 classes and a regularization parameter T = 2.

GMPCPP MT seeds were made as described above, spun down at 17,000 *g* for 20 min at RT, and resuspended with 100 µl of BRB80 mixed with 20 nM augmin holocomplex or octamer(H6ΔC). The MT/augmin mixture (5 µl) was applied to EM grids and stained likewise. The negative-stain data were collected with CM100 TEM (Philips) at 80 keV at a magnification of 64,000 and 130,000, respectively, for octamer(H6ΔC) and holocomplex with a defocus ranging from −2 to −4 µm. Images were recorded using ORCA camera with a calibrated pixel size of 7.0 Å.

In vitro pull-down assays for the interaction of γ-TuRC and augmin

Anti-GFP antibody–conjugated Dynabeads were preparedas in the ID experiments. 100 nM of each augmin complex was mixed with 10 nM γ-TuRC and the beads (20 µl) using a rotator for 2 h at 4°C. After incubation, beads were retrieved from solution and washed with three times of 150 µl TBS-T. Samples were eluted by boiling with SDS-PAGE sample buffer, followed by Western blot.

MT cosedimentation assay

For MT cosedimentation assays, 40 µM bovine tubulin was mixed with 1 mM DTT and 1 mM GTP in BRB80 and incubated at 37°C for 30 min. 50 µM Taxol was then added to the mixture, which was incubated for another 30 min. MTs were pelleted at 17,000 *g* for 20 min at RT and resuspended with BRB80Tx buffer (BRB80 with 50 µM Taxol). γ-TuRC and augmin were spun at 100,000 *g* for 15 min in the presence of 45% (wt/vol) sucrose cushion, and supernatants were collected for the following assay. MTs (2, 0.4, and 0.08 µM) were mixed respectively with 5 nM γ-TuRC and 5 nM γ-TuRC/50 nM augmin. 20-µl samples were loaded onto 80 µl of 45% (wt/vol) sucrose/BRB80Tx cushion and spun down at 100,000 *g* for 15 min at 22°C using a TLA-100 (Beckman Coulter) rotor. Supernatants were 30 µl from the top and pellets were 30 µl from the bottom of the tubes. Samples were loaded onto SDS-PAGE gels, followed by Western blot analyses.

IF of γ-TuRC on MTs

MTs were prepared in the same ways as previously mentioned. All reactions and buffers were at RT unless otherwise specified, and all incubations were performed in a humidity chamber. 60 nM MTs were mixed with 75 nM augmin holocomplex and 5 nM γ-TuRC in a 10-µl reaction at RT for 10 min. The mixture was then flown into a flow channel and allowed to adhere for 5 min. Unattached MTs were washed out by 20 µl BRB80, followed by fixation with −20°C methanol for ∼1 min and then by another wash in 20 µl of BRB80. The coverslips were washed with 50 µl blocking buffer (5% normal goat serum S1000 in BRB80; Vector Labs) and incubated for 1 h at 4°C. Reactions were incubated overnight at 4°C in blocking buffer with custom rabbit polyclonal anti–γ-TB at 1:100 dilution. The following day, reactions were subjected to three rounds of washing with 50 µl BRB80 each followed by a 15-min incubation. Reactions were incubated for 1 h in blocking buffer containing goat anti–rat IgG (H+L) secondary antibody and Alexa Fluor 568 conjugate (Thermo Fisher Scientific) at 1:2,500 dilution. Again, reactions were washed with 50 µl BRB80 three times, and each wash was followed by a 15-min incubation. Finally, reactions were mounted with ProLong Diamond Antifade Mountant (Life Technologies) and stored until imaging.

The images were acquired on Nikon TiE TIRF microscope using 1.49 NA oil-immersion objective and captured with an Andor Zyla sCMOS camera. To avoid bleaching in the red and infrared channels, random fields were located in the green channel and then imaged in all three channels using a multichannel acquisition function in the software. All adjustable imaging parameters (exposure time, laser intensity, and TIRF angle) were kept the same between reactions and experiments. Images from all experiments were collected in a single session.

Images were analyzed using MATLAB. To segment MTs, tubulin signal was first thresholded via Otsu method and further dilated to create a MT mask. MTs were isolated from the mask by finding connected components in the binary image, whereas small aggregates and false positives were eliminated by setting the minimum perimeter as 100 pixels. Mean γ-tubulin signal on each MT per pixel was calculated. The mean intensity from reverse mask of the entire field of view was subtracted from each MT and its corresponding γ-tubulin signal as background. Each experiment was repeated thrice, and at least 30 MTs were analyzed for each condition. Data from all three experiments were pooled and reported. Boxplots were generated using notBoxPlot function in MATLAB Central File Exchange (https://www.mathworks.com/matlabcentral/fileexchange/26508-notboxplot). P-values were calculated with the Wilcoxon rank-sum test in MATLAB.

Online supplemental material

The online supplemental material contains the quantification of MT nucleation kinetics in IgG and augmin add-back conditions (Fig. S1), which belong to Fig. 1 B. In addition, more experiments depict the purification of γ-TuRC, the weak interaction between augmin and γ-TuRC in solution, and the fact that augmin can target γ-TuRC to single MTs in vitro (Fig. S2 for Fig. 2). We show that augmin alone does not induce MT nucleation when added to extract or purified γ-TuRC (Fig. S3). All SDS-PAGE gels of the in vitro pull-down assays are depicted (Fig. S4 for Fig. 3). Finally, IP and IF experiments show that holocomplex, octamer, and T-III, but not T-II, bind to g-TuRC and recruit it along preexisting MTs (Fig. S5 for Fig. 5). Fig. S6 shows negative-stain analysis of augmin. Video 1 depicts that recombinant augmin can replace endogenous augmin in *Xenopus* egg extracts (for Fig. 1 B). In Video 2, different augmin complexes were added back to extracts (for Fig. 4 C).

Acknowledgments

We would like to thank Raymundo Alfaro-Aco for help in purifying γ-TuRC and Elbegduuren Erdenee for help in testing augmin subunit interactions. We are grateful to Dr. Martin Wuehr for support with the quantitative mass spectrometry experiments and Dr. Eva Nogales for the use of the University of California Berkeley EM facility. We also thank Dr. Gohta Goshima for critical reading of the manuscript and helpful comments.

This work was supported by a National Institutes of Health DP2 New Innovator Award (National Institute of General Medical Sciences,1DP2GM123493-01), the Pew Scholars Program in the Biomedical Sciences, and the David and Lucile Packard Foundation (all to S. Petry). R.S. Kadzik was supported by an National Institutes of Health postdoctoral fellowship (1F32GM119195-01) and A. Thawani was supported by an American Heart Association Graduate Research Fellowship (17PRE33660328).

The authors declare no competing financial interests.

Author contributions: J.-G. Song designed and conducted the experiments. M.R. King purified augmin antibodies and carried out IF experiments and quantification of the data (Fig. 2, C and D). R. Zhang performed negative staining EM and 2D class averaging (Fig. 5 C). R.S. King purified endogenous γ-TuRC and performed in vitro MT nucleation assays (Figs. S2 B and S3 B). A. Thawani analyzed MT nucleation kinetics (Fig. S1) and contributed to the quantification of IF data (Fig. 2 D). S. Petry contributed to the experimental design and oversaw the work. J.-G. Song and S. Petry wrote the manuscript. All authors reviewed the data and the manuscript.

Submitted: 13 November 2017
Revised: 10 March 2018
Accepted: 1 May 2018

References

Aitken, C.E., R.A. Marshall, and J.D. Puglisi. 2008. An oxygen scavenging system for improvement of dye stability in single-molecule fluorescence experiments. *Biophys. J.* 94:1826–1835. https://doi.org/10.1529/biophysj.107.117689

Alfaro-Aco, R., A. Thawani, and S. Petry. 2017. Structural analysis of the role of TPX2 in branching microtubule nucleation. *J. Cell Biol.* 216:983–997. https://doi.org/10.1083/jcb.201607060

Brinkley, B.R. 1985. Microtubule organizing centers. *Annu. Rev. Cell Biol.* 1:145–172. https://doi.org/10.1146/annurev.cb.01.110185.001045

Chen, J.W.C., Z.A. Chen, K.B. Rogala, J. Metz, C.M. Deane, J. Rappsilber, and J.G. Wakefield. 2017. Cross-linking mass spectrometry identifies new interfaces of Augmin required to localise the γ-tubulin ring complex to the mitotic spindle. *Biol. Open.* 6:654–663. https://doi.org/10.1242/bio.022905

Drozdetskiy, A., C. Cole, J. Procter, and G.J. Barton. 2015. JPred4: a protein secondary structure prediction server. *Nucleic Acids Res.* 43(W1):W389-94. https://doi.org/10.1093/nar/gkv332

Fong, K.W., Y.K. Choi, J.B. Rattner, and R.Z. Qi. 2008. CDK5RAP2 is a pericentriolar protein that functions in centrosomal attachment of the gamma-tubulin ring complex. *Mol. Biol. Cell.* 19:115–125. https://doi.org/10.1091/mbc.e07-04-0371

Goshima, G., R. Wollman, S.S. Goodwin, N. Zhang, J.M. Scholey, R.D. Vale, and N. Stuurman. 2007. Genes required for mitotic spindle assembly in Drosophila S2 cells. *Science.* 316:417–421. https://doi.org/10.1126/science.1141314

Goshima, G., M. Mayer, N. Zhang, N. Stuurman, and R.D. Vale. 2008. Augmin: A protein complex required for centrosome-independent microtubule generation within the spindle. *J. Cell Biol.* 181:421–429. https://doi.org/10.1083/jcb.200711053

Gruss, O.J., R.E. Carazo-Salas, C.A. Schatz, G. Guarguaglini, J. Kast, M. Wilm, N. Le Bot, I. Vernos, E. Karsenti, and I.W. Mattaj. 2001. Ran induces spindle assembly by reversing the inhibitory effect of importin alpha on TPX2 activity. *Cell.* 104:83–93. https://doi.org/10.1016/S0092-8674(01)00193-3

Hannak, E., and R. Heald. 2006. Investigating mitotic spindle assembly and function in vitro using Xenopus laevis egg extracts. *Nat. Protoc.* 1:2305–2314. https://doi.org/10.1038/nprot.2006.396

Haren, L., M.H. Remy, I. Bazin, I. Callebaut, M. Wright, and A. Merdes. 2006. NEDD1-dependent recruitment of the gamma-tubulin ring complex to the centrosome is necessary for centriole duplication and spindle assembly. *J. Cell Biol.* 172:505–515. https://doi.org/10.1083/jcb.200510028

Ho, C.M.K., T. Hotta, Z. Kong, C.J.T. Zeng, J. Sun, Y.R.J. Lee, and B. Liu. 2011. Augmin plays a critical role in organizing the spindle and phragmoplast microtubule arrays in Arabidopsis. *Plant Cell.* 23:2606–2618. https://doi.org/10.1105/tpc.111.086892

Hsia, K.C., E.M. Wilson-Kubalek, A. Dottore, Q. Hao, K.L. Tsai, S. Forth, Y. Shimamoto, R.A. Milligan, and T.M. Kapoor. 2014. Reconstitution of the augmin complex provides insights into its architecture and function. *Nat. Cell Biol.* 16:852–863. https://doi.org/10.1038/ncb3030

Kimanius, D., B.O. Forsberg, S.H.W. Scheres, and E. Lindahl. 2016. Accelerated cryo-EM structure determination with parallelisation using GPUs in RELION-2. *eLife.* 5:21. https://doi.org/10.7554/eLife.18722

King, M., and S. Petry. 2016. Visualizing and Analyzing Branching Microtubule Nucleation Using Meiotic Xenopus Egg Extracts and TIRF Microscopy. *In* Mitotic Spindle: Methods and Protocols. Vol. 1413. P. Chang, and R. Ohi, editors. Humana Press Inc, Totowa. 77–85. https://doi.org/10.1007/978-1-4939-3542-0_6

Kollman, J.M., A. Merdes, L. Mourey, and D.A. Agard. 2011. Microtubule nucleation by γ-tubulin complexes. *Nat. Rev. Mol. Cell Biol.* 12:709–721. https://doi.org/10.1038/nrm3209

Lander, G.C., S.M. Stagg, N.R. Voss, A. Cheng, D. Fellmann, J. Pulokas, C. Yoshioka, C. Irving, A. Mulder, P.W. Lau, et al. 2009. Appion: an integrated, database-driven pipeline to facilitate EM image processing. *J. Struct. Biol.* 166:95–102. https://doi.org/10.1016/j.jsb.2009.01.002

Lawo, S., M. Bashkurov, M. Mullin, M.G. Ferreria, R. Kittler, B. Habermann, A. Tagliaferro, I. Poser, J.R.A. Hutchins, B. Hegemann, et al. 2009. HAUS, the 8-subunit human Augmin complex, regulates centrosome and spindle integrity. *Curr. Biol.* 19:816–826. https://doi.org/10.1016/j.cub.2009.04.033

Lüders, J., and T. Stearns. 2007. Microtubule-organizing centres: a re-evaluation. *Nat. Rev. Mol. Cell Biol.* 8:161–167. https://doi.org/10.1038/nrm2100

Lüders, J., U.K. Patel, and T. Stearns. 2006. GCP-WD is a gamma-tubulin targeting factor required for centrosomal and chromatin-mediated microtubule nucleation. *Nat. Cell Biol.* 8:137–147. https://doi.org/10.1038/ncb1349

Mindell, J.A., and N. Grigorieff. 2003. Accurate determination of local defocus and specimen tilt in electron microscopy. *J. Struct. Biol.* 142:334–347. https://doi.org/10.1016/S1047-8477(03)00069-8

Moritz, M., M.B. Braunfeld, J.W. Sedat, B. Alberts, and D.A. Agard. 1995. Microtubule nucleation by gamma-tubulin-containing rings in the centrosome. *Nature.* 378:638–640. https://doi.org/10.1038/378638a0

Mullins, R.D., J.A. Heuser, and T.D. Pollard. 1998. The interaction of Arp2/3 complex with actin: nucleation, high affinity pointed end capping, and formation of branching networks of filaments. *Proc. Natl. Acad. Sci. USA.* 95:6181–6186. https://doi.org/10.1073/pnas.95.11.6181

Nilsson, B., T. Moks, B. Jansson, L. Abrahmsén, A. Elmblad, E. Holmgren, C. Henrichson, T.A. Jones, and M. Uhlén. 1987. A synthetic IgG-binding domain based on staphylococcal protein A. *Protein Eng.* 1:107–113. https://doi.org/10.1093/protein/1.2.107

Petry, S., A.C. Groen, K. Ishihara, T.J. Mitchison, and R.D. Vale. 2013. Branching microtubule nucleation in Xenopus egg extracts mediated by augmin and TPX2. *Cell.* 152:768–777. https://doi.org/10.1016/j.cell.2012.12.044

Reck-Peterson, S.L., A. Yildiz, A.P. Carter, A. Gennerich, N. Zhang, and R.D. Vale. 2006. Single-molecule analysis of dynein processivity and stepping behavior. *Cell.* 126:335–348. https://doi.org/10.1016/j.cell.2006.05.046

Rivero, S., J. Cardenas, M. Bornens, and R.M. Rios. 2009. Microtubule nucleation at the cis-side of the Golgi apparatus requires AKAP450 and GM130. *EMBO J.* 28:1016–1028. https://doi.org/10.1038/emboj.2009.47

Robinson, R.C., K. Turbedsky, D.A. Kaiser, J.B. Marchand, H.N. Higgs, S. Choe, and T.D. Pollard. 2001. Crystal structure of Arp2/3 complex. *Science.* 294:1679–1684. https://doi.org/10.1126/science.1066333

Suloway, C., J. Pulokas, D. Fellmann, A. Cheng, F. Guerra, J. Quispe, S. Stagg, C.S. Potter, and B. Carragher. 2005. Automated molecular microscopy: the new Leginon system. *J. Struct. Biol.* 151:41–60. https://doi.org/10.1016/j.jsb.2005.03.010

Thawani, A., R.S. Kadzik, and S. Petry. 2018. XMAP215 is a microtubule nucleation factor that functions synergistically with the γ-tubulin ring complex. *Nat. Cell Biol.* 20:575–585. https://doi.org/10.1038/s41556-018-0091-6

Uehara, R., R.S. Nozawa, A. Tomioka, S. Petry, R.D. Vale, C. Obuse, and G. Goshima. 2009. The augmin complex plays a critical role in spindle microtubule generation for mitotic progression and cytokinesis in human cells. *Proc. Natl. Acad. Sci. USA.* 106:6998–7003. https://doi.org/10.1073/pnas.0901587106

Wu, G., Y.T. Lin, R. Wei, Y. Chen, Z. Shan, and W.H. Lee. 2008. Hice1, a novel microtubule-associated protein required for maintenance of spindle integrity and chromosomal stability in human cells. *Mol. Cell. Biol.* 28:3652–3662. https://doi.org/10.1128/MCB.01923-07

Zheng, Y., M.L. Wong, B. Alberts, and T. Mitchison. 1995. Nucleation of microtubule assembly by a gamma-tubulin-containing ring complex. *Nature.* 378:578–583. https://doi.org/10.1038/378578a0